Phys Chem Minerals (2003) 30: 590 – 598
DOI 10.1007/s00269-003-0345-z

ORIGINAL PAPER

S. C. Tarantino · M. Zema
M. Pistorino · M. C. Domeneghetti

High-temperature X-ray investigation of natural columbites

Received: 3 April 2003 / Accepted: 30 June 2003

Abstract Structural investigations at high temperature were carried out on natural columbite samples across the join $Fe(Nb_{0.95}Ta_{0.05})_2O_6$–$Mn(Nb_{0.95}Ta_{0.05})_2O_6$. The samples were preliminarily annealed to attain the complete cation-ordered state and avoid the superimposition of the effects of cation ordering during high-temperature studies. Unit-cell parameters of three columbites with different X_{Fe} content were measured at regular intervals in the temperature range 25–900 °C using single-crystal X-ray diffraction techniques. The crystal structures of completely ordered ferrocolumbite and manganocolumbite were also refined from intensity data collected at room temperature, 300 and 600 °C. Structural thermal expansion coefficients show positive, linear expansion of *a*, *b*, *c* lattice constants and cell volume. In general, slightly higher expansion occurs along *a* and *c* directions. However, anisotropy decreases sharply with decreasing Fe content. Reversibility of thermal expansion in the investigated temperature range was checked by high-temperature diffraction studies under heating-up and cooling-down conditions. Impurities do not play an important role in thermal expansion of columbites; expansion coefficients measured on two crystals of the same sample characterized by different Ti content are in fact almost identical. Structural changes with temperature essentially affect bond lengths: volumes of both A and B octahedral sites increase linearly with temperature, whereas interpolyhedral geometrical parameters do not vary significantly.

Keywords Columbite · HT X-ray diffraction · Thermal expansion

S. C. Tarantino · M. Zema (✉) · M. Pistorino
M. C. Domeneghetti
Dipartimento di Scienze della Terra,
Università di Pavia, Via Ferrata 1,
27100 Pavia, Italy
e-mail: zema@crystal.unipv.it
Tel.: +39-0382-50-5869
Fax: +39-0382-50-5890

Introduction

Minerals of the columbite group occur as accessory phases in granitic pegmatites. They have the general formula AB_2O_6 where $A = Fe^{2+}$, Mn^{2+} and $B = Nb^{5+}$, Ta^{5+}, with other elements such as Ca^{2+}, Sc^{3+}, Fe^{3+}, Ti^{4+}, Sn^{4+}, W^{6+} and minor substitutions of rare-earth elements. In their crystal structure (space group *Pbcn*), cations may occupy two different octahedral sites, A and B, with divalent cations preferring the A site and pentavalent cations preferring the B site. An order–disorder process allows intracrystalline cation exchange between A and B sites. At present, the degree of cation order in samples of the columbite-group minerals is estimated qualitatively from the ratio of the *a* cell edge and the *c* cell edge (Nickel et al. 1963; Turnock 1966; Komkov 1970; Černý and Turnock 1971; Wise et al. 1985; Černý et al. 1986); a calibration of the degree of order as a function of these two lattice parameters has been given by Ercit et al. (1995): % order (± 5%) = 1727–941.6 (*c*–0.2329 *a*).

Natural columbite-group minerals show widely variable degrees of order; these minerals, crystallized as a disordered phase, are likely to have ordered subsequently during cooling of the parent rock (Černý and Ercit 1985; Černý et al. 1986; Mulja et al. 1996). Columbite-group minerals are then potential indicators of the evolutionary history of their parent rocks (Trueman and Černý 1982; Černý et al. 1986; Lahti 1987; Ercit 1994). To this purpose, fundamental information might be derived from the structural states of these minerals once the mechanisms driving the (Fe, Mn) versus (Nb, Ta) order–disorder process are known.

It has been shown so far from ex situ annealing experiments that in columbites cation ordering occurs upon heating (Nickel et al. 1963; Ercit et al. 1995) and no significant oxidation of Fe^{2+} is observed up to 1100 °C. Nevertheless, the high-temperature behaviour of columbite-group minerals is still unknown.

In the present work, the first in situ high-temperature data on cation-ordered natural columbites are presented.

Thermal expansion of three natural columbite samples with different composition has been measured in the temperature range 25–900 °C by means of single-crystal X-ray diffraction (SC-XRD). The crystal structures of completely ordered ferrocolumbite and manganocolumbite were also refined from intensity data collected at room temperature, 300 and 600 °C.

Experimental

Three natural columbite samples were used for the present study: sample BRA, from S. José de Safira, Minas Gerais (Brazil), provided by the Mineralogical Museum of the University of Florence, inv. No. 41248; sample KRA, from Kragero (Norway), provided by the Mineralogical Museum of the University of Rome, inv. No. 22522/49; sample AMB, from Ambatofotsikely (Madagascar), provided by the Mineralogical Museum of the University of Florence, inv. No. 5594.

Electron microprobe analyses

Chemical analyses were performed on different fragments from each sample at the Department of Earth Sciences of the University of Modena with a ARL-SEMQ electron microprobe operating in the wavelength-dispersive (WDS) mode. Operating conditions were 15 kV and 20 nA sample current. Counting times were 20 s for peak and 5 s for background. Standards used were: Nb metal (Nb–$L\alpha$), Ta metal (Ta–$M\alpha$), ilmenite (Fe–$K\alpha$, Ti–$K\alpha$), Sc metal (Sc–$K\alpha$), spessartine (Mn–$K\alpha$), cassiterite (Sn–$L\alpha$), anorthite (Ca–$K\alpha$) and W metal (W–$M\alpha$). X-ray counts were converted into oxide weight percentages using the PROBS correction program (Donovan and Rivers 1990). Analyses are precise to within 1% for major elements and 3–5% for minor elements, based on counting statistics of the instrument. Only the spot analyses which satisfied the following conditions were averaged: (1) total oxide amount = 100 ± 1.5; (2) total cation content = 3.000 ± 0.01 atoms on the basis of six oxygen atoms. The analyses and the formulae calculated on the basis of six oxygen atoms for the columbite samples are reported in Table 1.

The three samples under investigation show very similar Nb/(Nb + Ta) ratios and different Fe/(Fe + Mn) ratios, the latter being representative of $FeNb_2O_6$-$MnNb_2O_6$ solid solution (0.15 for sample KRA; 0.55 for AMB; 0.78 for BRA). Samples KRA and BRA are homogeneous. Sample AMB has two different compositions characterized by identical X_{Fe} but different Ti contents (Table 1). These compositions, labelled Col AMB/A and Col AMB/B, are internally homogeneous. Further electron microprobe work should be done to establish the spatial constraints of compositional inhomogeneity of sample AMB, but this is beyond the scope of the present work.

On the basis of their chemical compositions, theoretical unit-cell parameters for the corresponding ordered columbites were calculated using Eq. (3), (4) and (5) in Ercit et al. (1995). These are reported in Table 1.

Table 1 Electron microprobe analyses

	Col BRA	Col AMB/A	Col AMB/B	Col KRA
oxide (wt%)				
MnO	4.42(54)[a]	7.32(48)	8.40(24)	15.97(15)
FeO	15.52(39)	13.46(10)	10.27(9)	2.82(9)
TiO_2	0.62(13)	5.46(35)	4.27(67)	1.73(6)
Sc_2O_3	0.05(2)	1.92(5)	0.86(2)	0.03(2)
CaO	0.01(1)	0.09(1)	0.01(1)	0.13(1)
SnO	0.02(2)	0.36(2)	0.20(1)	0.11(1)
Ta_2O_5	5.99(37)	2.74(31)	5.70(22)	10.43(46)
WO_3	0.20(10)	0.06(3)	0.23(23)	0.07(10)
Nb_2O_5	72.86(55)	67.46(45)	69.23(61)	67.82(54)
Total	99.68(77)	99.23(32)	99.17(22)	99.11(6)
Atoms per formula unit (based on six oxygen atoms)				
Mn	0.215(25)	0.349(10)	0.404(11)	0.792(5)
Fe	0.747(23)	0.449(4)	0.488(2)	0.138(5)
Ti	0.027(6)	0.468(12)	0.182(28)	0.077(2)
Sc	0.003(1)	0.037(1)	0.043(1)	0.002(1)
Ca	0.001(1)	0.004(1)	0.001(1)	0.009(1)
Sn	0.001(1)	0.001(1)	0.005(1)	0.003(1)
Ta	0.094(5)	0.085(6)	0.088(4)	0.166(8)
W	0.003(1)	0.003(2)	0.004(4)	0.001(1)
Nb	1.894(7)	1.592(11)	1.776(17)	1.794(8)
Total	2.983(2)	2.989(1)	2.989(2)	2.979(1)
X_{Fe}[b]	0.78	0.56	0.55	0.15
X_{Nb}	0.95	0.95	0.95	0.92
Expected unit-cell parameters for corresponding ordered columbites[b c]				
a (Å)	14.2939	14.3047	14.3247	14.3955
b (Å)	5.7360	5.7328	5.7402	5.7545
c (Å)	5.0573	5.0626	5.0642	5.0782

[a] Standard deviations are given in parentheses
[b] X_{Fe} = Fe / (Fe + Mn); X_{Nb} = Nb / (Nb + Ta)
[c] Theoretical values are calculated using Eq. (3), (4) and (5) in Ercit et al. (1995)

Crystal selection and preparation

A preliminary selection based on shape and morphology of the crystals was carried out by optical microscope. Crystals showing sharp, narrow X-ray diffraction profiles were selected. Size, lattice constants and ordering degree *Q* calculated on the basis of unit-cell parameters from Ercit et al (1995) are reported for each crystal in Table 2. Selected columbite crystals were labelled Col KRA N.5, Col BRA N.3, Col AMB N.1 and Col AMB N.12. The two crystals from sample AMB are characterized by different lattice constants, and may be considered representative of the two different compositions.

As already mentioned above, it is known that heat treatment induces cation ordering in columbites. In order to avoid the superimposition of the effects of cation ordering on unit-cell parameters during high-temperature studies, the four crystals were preliminarily ordered by heating under vacuum at 950 °C for 15 h. Complete ordered cation distribution is stable over the *T*, *P* conditions of this study. Unit-cell parameters of ordered crystals, measured at room temperature, are reported in Tables 3–6. They are in good agreement with the values calculated on the basis of chemical composition using Eq. (3), (4) and (5) in Ercit et al. (1995), and reported in Table 1. Crystals Col AMB N.1 and Col AMB N.12 can actually be referred to the two different compositions: crystal Col AMB N.1 is likely to have composition Col AMB/A, characterized by higher Ti content, while crystal Col

Table 2 Details of natural columbite crystals studied. Standard deviations are given in parentheses

Samples	Size (mm)	*a* (Å)	*b* (Å)	*c* (Å)	*V* (Å^3)	*Q* (%)
Col BRA N.3	0.198 × 0.198 × 0.247	14.2427(43)	5.7275(17)	5.0861(25)	414.9(3)	61.3(3)
Col AMB N.1	0.165 × 0.165 × 0.165	14.1870(87)	5.7165(36)	5.1223(36)	415.4(5)	15.0(4)
Col AMB N.12	0.112 × 0.224 × 0.308	14.2466(85)	5.7246(46)	5.0996(29)	415.9(5)	49.5(3)
Col KRA N. 5	0.165 × 0.198 × 0.231	14.3110(98)	5.7461(69)	5.1330(44)	422.1(7)	32.2(5)

Table 3 Unit-cell parameters of sample Col BRA N.3. Standard deviation are given in parentheses

T (°C)	a (Å)	b (Å)	c (Å)	V (Å^3)
RT	14.2880 (66)	5.7364 (36)	5.0562 (28)	414.41 (40)
50	14.2882 (70)	5.7366 (37)	5.0572 (28)	414.52 (41)
75	14.2931 (67)	5.7383 (35)	5.0595 (29)	414.97 (40)
100	14.2981 (63)	5.7403 (33)	5.0617 (27)	415.44 (37)
150	14.3031 (68)	5.7421 (33)	5.0637 (29)	415.88 (39)
200	14.3080 (63)	5.7433 (29)	5.0661 (26)	416.31 (35)
250	14.3139 (70)	5.7457 (35)	5.0687 (28)	416.87 (40)
300	14.3191 (56)	5.7482 (30)	5.0713 (22)	417.41 (33)
350	14.3240 (66)	5.7502 (34)	5.0731 (29)	417.85 (39)
400	14.3288 (65)	5.7527 (36)	5.0755 (25)	418.37 (38)
450	14.3352 (58)	5.7546 (31)	5.0774 (27)	418.85 (36)
500	14.3409 (64)	5.7565 (31)	5.0791 (28)	419.30 (37)
550	14.3460 (64)	5.7589 (33)	5.0810 (25)	419.78 (37)
600	14.3515 (60)	5.7610 (30)	5.0833 (28)	420.28 (36)
650	14.3574 (60)	5.7630 (29)	5.0851 (23)	420.75 (33)
700	14.3620 (55)	5.7648 (28)	5.0871 (27)	421.18 (34)
750	14.3688 (59)	5.7667 (28)	5.0893 (25)	421.70 (34)
800	14.3733 (61)	5.7692 (28)	5.0917 (26)	422.22 (35)
850	14.3789 (78)	5.7711 (35)	5.0934 (31)	422.66 (43)
900	14.2880 (66)	5.7364 (36)	5.0562 (28)	414.41 (40)
R^{2a}	0.9990	0.9983	0.9987	0.9996

[a] Statistic tests R^2 refers to linear regressions reported in Fig. 1a–d

AMB N.12 can be referred to the chemical composition indicated as Col AMB/B. The a and b lattice parameters for these crystals are significantly lower than those expected on the basis of Ercit's equations, probably because contraction of these lattice parameters caused by the presence of Ti is underestimated when this element is contained in a great amount.

The four crystals were put in silica tubes and held in place with quartz wool. The use of quartz wool instead of cements or glues avoids any mechanical stress during heat treatment. A small piece of graphite was used to prevent oxidation of Fe.

Measurement of lattice constants

Structural thermal expansion of the four ordered columbite crystals was measured by in situ X-ray single crystal diffraction in the 25–900 °C temperature range. The experiments were performed using a conventional Philips PW 1100 four-circle diffractometer equipped with a microfurnace for in situ high-temperature experiments. Operating conditions were 55 kV and 25 mA, with Mo–$K\lambda$ ($\lambda = 0.71073$ Å) incident radiation. For each crystal, unit cell parameters were measured from room temperature up to 900 °C at intervals of 50 °C. At each temperature, lattice constants (Tables 3–6) were derived from a least-squares procedure based on the Philips LAT routine and improved by Canillo et al. (1983) which allows taking into account up to 60 d^*-spacings, each measured considering all the reflections in the range $3° < \theta < 25°$. For crystal Col AMB N.1, the reversibility of thermal expansion was checked by measuring lattice parameters while the crystal was cooled from 875 °C down to room temperature.

SC-XRD data collection and structure refinements

Crystals Col KRA N.5 and Col BRA N.3 were used for X-ray single-crystal diffraction analyses at room temperature, 300 and 600 °C. Intensity data at room temperature were obtained on a Bruker AXS SMART APEX three-circle diffractometer equipped with a CCD detector whereas a conventional Philips PW1100 four-circle diffractometer equipped with a microfurnace for in situ heating was used for HT intensity data collection. Graphite-monochromatized Mo–$K\alpha$ radiation was used in both cases.

CCD data collections were carried out with operating conditions 50 kV and 30 mA. The Bruker SMART system of programs was used for preliminary crystal lattice determination and X-ray data collection. A total of 5400 frames (resolution: 512×512 pixels) were collected with six different goniometer settings using the ω scan mode (scan width: 0.2°ω; exposure time: 5 s.frame^{-1}; detector–sample distance: 5 cm). Completeness of measured data was achieved up to 35.8°θ. The Bruker program SAINT+ was used for data reduction including intensity integration, background and Lorentz-polarization corrections. Final unit-cell parameters (Table 7) were obtained by a least-squares procedure based on the positions of all measured reflections. These values are in good agreement with those gained by the conventional diffractometer (see Tables 3 and 6), within the uncertainties of both sets of measurements. The semi-empirical absorption correction of Blessing (1995), based on the determination of transmission factors for equivalent reflections, was applied using the program SADABS (Sheldrick 1996). Details on CCD data collections at room temperature on samples Col BRA N.3 and Col KRA N.5 are reported in Table 7.

High-temperature intensity data were collected with operating conditions 55 kV and 30 mA. Horizontal and vertical apertures were 2.0° and 1.5°, respectively. The equivalent reflections hkl and $\bar{h}kl$ were measured in the ω-2θ scan mode in the 2–26°θ range. The microfurnace itself limits the angular region to these values. Three standard reflections were collected every 200 reflections. X-ray diffraction intensities were obtained by measuring step-scan profiles and analyzing them by the Lehman and Larsen (1974) σ_I / I method, as modified by Blessing et al. (1974). Unit-cell parameters were derived by the Philips LAT routine, as described above. Intensities were corrected for absorption using the semi-empirical ψ scan method of North et al. (1968). Relevant parameters on data collections performed at high temperature by means of conventional diffractometer are reported in Table 7.

Structure refinements were carried out in space group *Pbcn* by full-matrix least-squares using SHELXL-97 (Sheldrick 1998). Although intensity data collections at room temperature were carried out in a wider θ range, structural data presented here refer to a set of data limited to 26°θ to guarantee internal consistency. This validates comparisons of crystal structures at different temperatures, in particular with respect to anisotropic displacement parameters. Equivalent reflections were averaged, and the resulting internal agreement factors R_{int} are reported in Table 7. Divalent cations (Fe^{2+} for sample Col BRA; Mn^{2+} for sample Col KRA) and pentavalent cations were considered fully ordered at the A and B sites, respectively. The Nb/Ta ratio was constrained on the basis of electron microprobe analyses and not

Table 4 Unit-cell parameters of sample Col AMB N.1. Standard deviation are given in parentheses

T (°C)	a (Å)	b (Å)	c (Å)	V (Å^3)
RT	14.2717 (88)	5.7158 (42)	5.0603 (31)	412.79 (47)
50	14.2726 (103)	5.7163 (45)	5.0609 (30)	412.90 (50)
75	14.2754 (88)	5.7172 (41)	5.0617 (27)	413.11 (45)
100	14.2784 (92)	5.7180 (43)	5.0628 (30)	413.35 (48)
150	14.2843 (92)	5.7204 (41)	5.0647 (33)	413.85 (48)
200	14.2904 (86)	5.7231 (42)	5.0662 (28)	414.34 (46)
250	14.2976 (79)	5.7238 (36)	5.0687 (28)	414.81 (42)
300	14.3012 (79)	5.7265 (36)	5.0709 (24)	415.29 (40)
350	14.3095 (73)	5.7281 (34)	5.0724 (25)	415.77 (38)
400	14.3143 (84)	5.7302 (36)	5.0742 (29)	416.21 (43)
450	14.3210 (83)	5.7320 (38)	5.0765 (27)	416.72 (43)
500	14.3251 (81)	5.7340 (26)	5.0784 (24)	417.14 (36)
550	14.3287 (75)	5.7364 (43)	5.0809 (23)	417.63 (43)
600	14.3340 (86)	5.7380 (49)	5.0832 (22)	418.09 (47)
650	14.3399 (77)	5.7406 (42)	5.0848 (22)	418.58 (42)
700	14.3452 (87)	5.7428 (40)	5.0865 (23)	419.03 (43)
750	14.3495 (93)	5.7441 (48)	5.0891 (22)	419.47 (48)
800	14.3577 (86)	5.7466 (50)	5.0909 (28)	420.04 (50)
850	14.3645 (92)	5.7480 (48)	5.0930 (23)	420.51 (48)
900	14.3685 (77)	5.7493 (39)	5.0946 (20)	420.86 (40)
R^{2a}	0.9983		0.9989	
Reversal experiment				
875	14.3643 (81)	5.7480 (44)	5.0940 (20)	420.59 (43)
825	14.3574 (96)	5.7459 (46)	5.0912 (25)	420.00 (48)
775	14.3524 (104)	5.7438 (55)	5.0884 (28)	419.47 (55)
725	14.3457 (91)	5.7416 (50)	5.0871 (23)	419.01 (49)
675	14.3421 (89)	5.7401 (49)	5.0845 (21)	418.58 (47)
625	14.3338 (86)	5.7385 (35)	5.0825 (28)	418.06 (43)
575	14.3286 (78)	5.7361 (45)	5.0805 (19)	417.57 (43)
525	14.3230 (82)	5.7344 (34)	5.0786 (23)	417.12 (39)
475	14.3161 (101)	5.7325 (42)	5.0762 (22)	416.59 (46)
425	14.3111 (98)	5.7307 (44)	5.0748 (28)	416.20 (49)
375	14.3073 (89)	5.7283 (38)	5.0726 (21)	415.73 (42)
325	14.3012 (88)	5.7264 (39)	5.0707 (23)	415.26 (43)
275	14.2962 (94)	5.7247 (47)	5.0691 (18)	414.86 (46)
225	14.2893 (86)	5.7227 (34)	5.0670 (22)	414.35 (39)
175	14.2847 (84)	5.7213 (33)	5.0650 (17)	413.95 (37)
125	14.2786 (90)	5.7188 (32)	5.0632 (25)	413.44 (40)
75	14.2723 (84)	5.7168 (38)	5.0615 (24)	412.98 (42)
RT	14.2708 (96)	5.7157 (40)	5.0598 (29)	412.72 (47)
R^{2a}	0.9987	0.9995	0.9982	0.9993

[a] Statistic tests R^2 refers to linear regressions reported in Figs. 1a–d and 2a–d

refined. The atomic scattering curves were taken from the International Tables for X-ray Crystallography (Ibers and Hamilton 1974). Structure factors were weighted according to $w = 1/[\sigma^2(F_o^2) + (AP)^2 + BP]$, where $P = (F_o^2 + 2F_c^2)/3$, and A and B were chosen for every crystal to produce a flat analysis of variance in terms of F_c^2 as suggested by the program. An extinction parameter x was refined to correct the structure factors according to the equation: $F_o = F_c\, k[1 + 0.001x F_c^2 \lambda^3 / \sin 2\theta]^{-1/4}$ (where k is the overall scale factor). All parameters were refined simultaneously. Highest correlation coefficients were 0.73 for crystal Col KRA N.5 and 0.81 for crystal Col BRA N.3, and were shown, in both cases, by overall scale factor and secondary extinction parameter. All final difference-Fourier maps were featureless. The values of the conventional agreement indices, R_1 and R_{all}, as well as the goodness of fit (S) are reported in Table 7. Anisotropic displacement parameters U_{ij} are reported in Tables 8 and 9 for crystals Col BRA N.5 and Col KRA N.3, respectively. Interatomic distances and selected geometrical parameters are reported in Table 10. Observed and calculated structure factors are available from the authors.

Table 5 Unit-cell parameters of sample Col AMB N.12. Standard deviation are given in parentheses

T (°C)	a (Å)	b (Å)	c (Å)	V (Å^3)
RT	14.3151 (91)	5.7355 (46)	5.0675 (34)	416.06 (51)
50	14.3166 (82)	5.7353 (44)	5.0676 (31)	416.10 (47)
75	14.3238 (89)	5.7351 (50)	5.0693 (31)	416.44 (51)
100	14.3262 (82)	5.7389 (57)	5.0715 (36)	416.96 (56)
150	14.3319 (93)	5.7406 (55)	5.0736 (34)	417.42 (56)
200	14.3383 (77)	5.7434 (51)	5.0757 (34)	417.99 (52)
250	14.3445 (72)	5.7447 (52)	5.0775 (34)	418.41 (52)
300	14.3493 (81)	5.7472 (50)	5.0801 (36)	418.95 (53)
350	14.3559 (73)	5.7489 (44)	5.0820 (28)	419.42 (45)
400	14.3600 (76)	5.7519 (45)	5.0842 (29)	419.94 (46)
450	14.3669 (88)	5.7538 (53)	5.0866 (35)	420.48 (55)
500	14.3716 (92)	5.7551 (51)	5.0883 (36)	420.85 (55)
550	14.3789 (88)	5.7581 (54)	5.0910 (32)	421.51 (54)
600	14.3834 (78)	5.7597 (47)	5.0923 (26)	421.87 (47)
650	14.3886 (82)	5.7623 (54)	5.0940 (31)	422.35 (53)
700	14.3945 (76)	5.7639 (50)	5.0950 (34)	422.72 (51)
750	14.4019 (75)	5.7642 (42)	5.0965 (30)	423.09 (45)
800	14.4055 (87)	5.7640 (45)	5.0986 (32)	423.35 (50)
850	14.4089 (87)	5.7664 (44)	5.1003 (33)	423.77 (50)
900	14.3151 (91)	5.7355 (46)	5.0675 (34)	416.06 (51)
R^{2a}	0.9988	0.9877	0.9960	0.9970

[a] Statistic tests R^2 refers to linear regressions reported in Fig. 1a–d

Table 6 Unit-cell parameters of sample Col KRA N.5. Standard deviation are given in parentheses

T (°C)	a (Å)	b (Å)	c (Å)	V (Å^3)
RT	14.3860 (121)	5.7478 (67)	5.0797 (42)	420.03 (70)
50	14.3892 (125)	5.7485 (78)	5.0807 (44)	420.26 (77)
100	14.3936 (104)	5.7513 (63)	5.0826 (38)	420.75 (64)
150	14.3994 (116)	5.7534 (72)	5.0846 (40)	421.24 (71)
200	14.4045 (121)	5.7552 (73)	5.0864 (42)	421.67 (73)
250	14.4105 (105)	5.7576 (66)	5.0887 (43)	422.21 (68)
300	14.4159 (118)	5.7593 (64)	5.0905 (48)	422.64 (71)
350	14.4239 (136)	5.7612 (81)	5.0923 (41)	423.16 (79)
400	14.4282 (122)	5.7640 (62)	5.0940 (48)	423.64 (70)
450	14.4355 (124)	5.7663 (64)	5.0962 (48)	424.20 (72)
500	14.4401 (132)	5.7685 (65)	5.0985 (48)	424.69 (73)
550	14.4434 (121)	5.7721 (58)	5.1005 (48)	425.22 (69)
600	14.4508 (127)	5.7741 (68)	5.1025 (48)	425.75 (74)
650	14.4596 (114)	5.7751 (59)	5.1040 (44)	426.21 (66)
700	14.4651 (119)	5.7788 (66)	5.1055 (42)	426.77 (70)
750	14.4722 (130)	5.7806 (75)	5.1082 (41)	427.34 (76)
800	14.4807 (134)	5.7815 (89)	5.1099 (44)	427.80 (85)
850	14.4841 (128)	5.7846 (62)	5.1126 (46)	428.36 (71)
900	14.4936 (143)	5.7867 (71)	5.1146 (41)	428.96 (76)
R^{2a}	0.9970	0.9980	0.9993	0.9994

[a] Statistic tests R^2 refers to linear regressions reported in Fig. 1a–d

Results and discussion

High-temperature thermal expansion

In situ high-temperature single-crystal X-ray diffraction measurements show that in the temperature range 25–900 °C, the four columbite crystals are characterized by relatively low positive expansions of a, b, c lattice constants and cell volume (Fig. 1a–d). All the expansion

Table 7 Details on data collection and structure refinements

	Col KRA N.5			Col BRA N.3		
T (°C)	25	300	600	25	300	600
a (Å)	14.3869 (3)	14.419 (12)	14.4602 (59)	14.2891 (4)	14.3139 (54)	14.3485 (58)
b (Å)	5.7471 (1)	5.7583 (35)	5.7737 (45)	5.7379 (2)	5.7464 (26)	5.7588 (28)
c (Å)	5.0806 (1)	5.0913 (26)	5.1037 (21)	5.0584 (1)	5.0697 (20)	5.0829 (21)
I_{meas}[a]	6215[d]	815	816	6147[d]	802	814
I_{ind}[b]	416	419	421	410	411	417
I_{obs}[c]	400	281	312	394	281	296
R_{int}%	1.93	6.55	5.53	1.97	5.10	7.91
R_1%	2.25	2.82	3.80	1.96	3.68	5.84
R_{all}%	2.35	5.83	5.72	2.00	5.66	7.60
S	1.220	1.051	1.114	1.223	1.127	1.050

[a] I_{meas} = number of measured reflections
[b] I_{ind} = number of independent reflections
[c] I_{obs} = number of reflections with $F_o > 4\sigma F_o$ used for calculation of the conventional index R_1
[d] After merging identical reflections. Redundancy in measured intensity data was ~ 1.7 for both crystals

Table 8 Anisotropic displacement parameters U_{ij} ($\times 10^{-4}$) for crystal Col BRA N.3. Standard deviations are given in parentheses

RT						300 °C					600 °C				
	A	B	O1	O2	O3	A	B	O1	O2	O3	A	B	O1	O2	O3
U_{11}	61(5)	49(3)	81(9)	85(8)	84(9)	195(10)	169(7)	213(23)	239(22)	242(22)	257(15)	202(9)	241(26)	287(26)	231(24)
U_{22}	71(5)	52(3)	57(9)	77(9)	72(8)	160(10)	125(6)	194(21)	212(21)	171(22)	270(15)	183(9)	191(24)	285(28)	233(26)
U_{33}	75(5)	63(3)	88(8)	114(8)	81(8)	284(10)	216(6)	243(21)	228(20)	238(18)	369(14)	290(8)	321(26)	371(29)	336(23)
U_{23}	0(0)	−1(1)	12(6)	−2(6)	−9(6)	0(0)	−1(2)	28(23)	−6(22)	18(22)	0(0)	−2(2)	16(23)	−6(27)	21(23)
U_{13}	−2(2)	−3(1)	−3(6)	−3(6)	−3(7)	−5(5)	−2(2)	3(20)	8(20)	17(22)	4(6)	−6(2)	19(22)	−43(25)	15(23)
U_{12}	0(0)	3(1)	12(6)	13(6)	−14(6)	0(0)	−1(2)	−31(23)	4(22)	−14(20)	0(0)	2(3)	33(25)	56(26)	−27(24)
U_{eq}	69(3)	55(2)	75(5)	92(5)	79(5)	213(6)	170(4)	217(12)	226(12)	217(13)	299(8)	225(5)	251(15)	314(16)	267(15)

Table 9 Anisotropic displacement parameters U_{ij} ($\times 10^{-4}$) for crystal Col KRA N.5. Standard deviations are given in parentheses

RT						300 °C					600 °C				
	A	B	O1	O2	O3	A	B	O1	O2	O3	A	B	O1	O2	O3
U_{11}	63(6)	82(3)	104(15)	111(16)	92(15)	134(10)	116(5)	167(31)	245(31)	201(26)	210(12)	172(6)	263(36)	351(38)	273(33)
U_{22}	82(6)	62(3)	73(15)	89(15)	59(13)	178(8)	129(4)	189(27)	203(27)	168(31)	260(13)	180(6)	211(33)	198(32)	249(36)
U_{33}	61(5)	71(3)	88(14)	103(15)	91(13)	160(6)	126(3)	183(21)	168(20)	151(15)	236(11)	177(5)	253(33)	264(33)	233(28)
U_{23}	0(0)	−1(1)	19(12)	−4(13)	−14(12)	0(0)	−2(3)	13(23)	53(23)	53(21)	0(0)	−3(3)	29(31)	−28(34)	−16(32)
U_{13}	3(3)	5(1)	15(12)	11(12)	16(12)	12(6)	−8(2)	−7(21)	0(22)	4(25)	11(8)	−8(3)	30(29)	−33(32)	16(31)
U_{12}	0(0)	2(1)	14(12)	14(12)	−3(12)	0(0)	6(3)	−7(28)	62(26)	2(28)	0(0)	1(3)	6(32)	43(32)	−19(33)
U_{eq}	69(3)	72(2)	88(8)	101(9)	80(9)	158(5)	124(2)	180(15)	205(15)	173(16)	235(7)	176(3)	242(19)	271(20)	252(20)

curves could be fitted linearly, the validity of which is shown by high R^2 statistical tests (Tables 3–6). Slight scattering of data, but no significant deviation from linearity, was observed for the b cell parameter in sample Col AMB N.12 above 700 °C.

In Fig. 2a–d variations of lattice parameters and cell volume for crystal Col AMB N.1 under heating-up and cooling-down conditions are reported. The almost perfect superimposition of the curves (differences are well within the uncertainties of both measurements) proves that thermal expansion is reversible in the temperature range 25–900 °C. It is worth noting that, for each parameter, the slopes of all the linear fits are very similar, thus indicating that differences in divalent cations content as well as the presence of impurities (e.g. Ti) have not a strong effect on thermal expansion of columbites.

Thermal expansion coefficients were calculated from the data reported in Fig. 1a–d. The values of $\alpha_x = (1/x_0) \cdot (\delta x/\delta T)_P$, where x represents a, b and c cell parameters, and $\alpha_V = (1/V_0) \cdot (\delta V/\delta T)_P$ are presented in Table 11. Mean thermal expansion coefficients were calculated on the basis of $\bar{\alpha} = [\alpha(a) - \alpha(b) + \alpha(c)]/3$. These data indicate similar expansion effects for all the columbites under investigation [$\bar{\alpha}$ ranges between 7.18(22) and 7.73(16)]. However, slightly higher expansion occurs in general along a and c directions. In particular, for the ferrocolumbite BRA, the order of axial

Table 10 Bond distances (Å) and selected geometrical parameters. Standard deviations are given in parentheses

	Col BRA N.3			Col KRA N.5		
T (°C)	25	300	600	25	300	600
Site A						
A–O1 (×2)	2.1065(17)	2.1105(44)	2.1233(50)	2.1394(31)	2.1437(50)	2.1436(66)
A–O2 (×2)	2.1311(17)	2.1378(46)	2.1286(52)	2.1583(32)	2.1635(49)	2.1729(67)
A–O2 (×2)	2.1657(16)	2.1745(42)	2.1923(51)	2.2199(33)	2.2334(53)	2.2432(68)
Average	2.1341	2.1409	2.1481	2.1725	2.1802	2.1866
ELD[a]	4.59	4.59	4.6	5.24	5.21	5.32
Ct(A)–A	0.2232(6)	0.2259(12)	0.2328(18)	0.2669(10)	0.2741(18)	0.2851(23)
Site B						
B–O1	1.9201(16)	1.9290(44)	1.9206(49)	1.9210(31)	1.9218(48)	1.9266(66)
B–O1	2.0782(16)	2.0772(42)	2.0878(47)	2.0636(30)	2.0699(48)	2.0823)64)
B–O2	1.8000(16)	1.7979(42)	1.8037(48)	1.7939(32)	1.7931(50)	1.7978(66)
B–O3	2.0670(16)	2.0706(43)	2.0664(50)	2.0621(31)	2.0720(46)	2.0760(64)
B–O3	1.9537(16)	1.9545(41)	1.9635(47)	1.9539(31)	1.9476(51)	1.9575(65)
B–O3	2.2767(16)	2.2831(41)	2.2927(47)	2.2798(31)	2.2933(50)	2.2929(67)
Average	2.0160	2.0187	2.0225	2.0124	2.0163	2.0222
ELD[a]	3.39	3.32	3.35	3.65	3.39	3.37
Ct(B)–B	0.3306(3)	0.3292(6)	0.3317(8)	0.3271(4)	0.3271(6)	0.3261(8)
Interpolyhedral geometrical parameters						
A–A	3.2018(5)	3.2124(15)	3.2280(19)	3.2783(16)	3.2920(21)	3.3126(25)
B–B	3.2672(3)	3.2700(12)	3.2791(14)	3.2735(14)	3.2770(15)	3.2867(17)
Ct(A)–Ct(A)[b]	2.9493	2.9564	2.9637	2.9698	2.9748	2.9816
Ct(B)–Ct(B)	2.9161	2.9213	2.9275	2.9258	2.9308	2.9399
O2–O2–O2 (°)[c]	124.0(1)	124.0(3)	123.7(3)	124.5(2)	124.2(4)	124.5(5)
O1–O1–O1 (°)	129.7(1)	130.0(3)	130.0(4)	132.0(2)	131.7(4)	131.6(5)
O3–O3–O3 (°)	60.73(4)	60.89(9)	60.95(11)	61.14(8)	61.2(1)	61.1(2)

[a] ELD (edge length distortion) is defined as $\mathrm{ELD} = \frac{100}{n}\sum_{i=1}^{n}\frac{(x-x)_i-(x-x)_m}{(x-x)_m}\%$, where m = average (Griffen and Ribbe 1979)

[b] Ct(A) and Ct(B) are the centroids of polyhedra A and B, respectively

[c] Angles O2–O2–O2, O1–O1–O1 and O3–O3–O3 are indicative of the extension of the chains

thermal expansion coefficients is $\alpha(c) > \alpha(a) > \alpha(b)$, while for the two crystals from sample AMB it is $\alpha(c) \sim \alpha(a) > \alpha(b)$; and in the manganocolumbite KRA, expansion along the three axes is almost identical, hence $\alpha(c) \sim \alpha(a) \sim \alpha(b)$. Quantitative estimations of structure-controlled thermal expansion anisotropies were derived using the formalism of Schneider and Eberhard (1990):

$$A = (|\alpha(b) - \alpha(c)| + \alpha(b) - \alpha(a)| + |\alpha(c) - \alpha(a)|) \times 10^{-6},$$

and are reported in Table 11. These values show that anisotropy decreases sharply with decreasing Fe content.

Axial thermal expansion coefficients for the two crystals from sample AMB are all within estimated standard deviations. This suggests that minor variations in impurity content do not play an important role in thermal expansion of the columbite structure.

HT structural model

Refinements of room- and high-temperature diffraction data allowed analysis of the thermal structural modifications to be improved. To the best of our knowledge, there are no previous single-crystal structural data available for columbite-group minerals at high temperature.

Columbite-group minerals crystallize in the orthorhombic system, space group *Pbcn*, with an α-PbO_2-type derived structure. NbO_6 octahedra share edges and form zig-zag chains along the *c* axis; the octahedra of adjacent chains share corners to form double layers parallel to the *bc* plane. The double layers are linked together along the [100] direction through AO_6 units. These AO_6 octahedra also share edges to form zig-zag chains along the *c* axis. In the cation-ordered structure the A position is occupied by Mn^{2+} and Fe^{2+}. Because Mn^{2+} is larger than Fe^{2+}, the A site in manganocolumbite is significantly larger than in ferrocolumbite. Hence ferrocolumbite is more "compact" and is expected to expand largely with temperature. The data in Table 11 confirm that the highest axial thermal expansion coefficient is shown by the ferrocolumbite BRA along the *c* direction, corresponding to the direction of extension of the chains. Beyond this general standpoint, the average thermal expansion coefficient as well as the differences in axial expansivities are probably due to the complex interplay of internal strains within the structures arising from the relative expansion of the A and B polyhedra.

Table 10 shows selected bond lengths and other geometrical parameters determined for crystals Col BRA N.3 and Col KRA N.5 at 25, 300 and 600 °C. Examination of this table shows that heat treatment of columbites results in a general expansion of both A and B sites, with minor internal distortions and negligible modification of the extension of the octahedral chains. As evident from Fig. 3a, average <A–O> bond lengths vary linearly as a function of temperature. It is worth noting that the slopes of linear regressions and hence the linear thermal expansion coefficients of bond lengths for the A polyhedron are identical for the two samples analyzed. With increasing temperature, an out-of-centre displacement of the divalent cation occurs because of the expansion of the A site. Manganocolumbite shows a larger cation–centroid distance and a steeper increase of

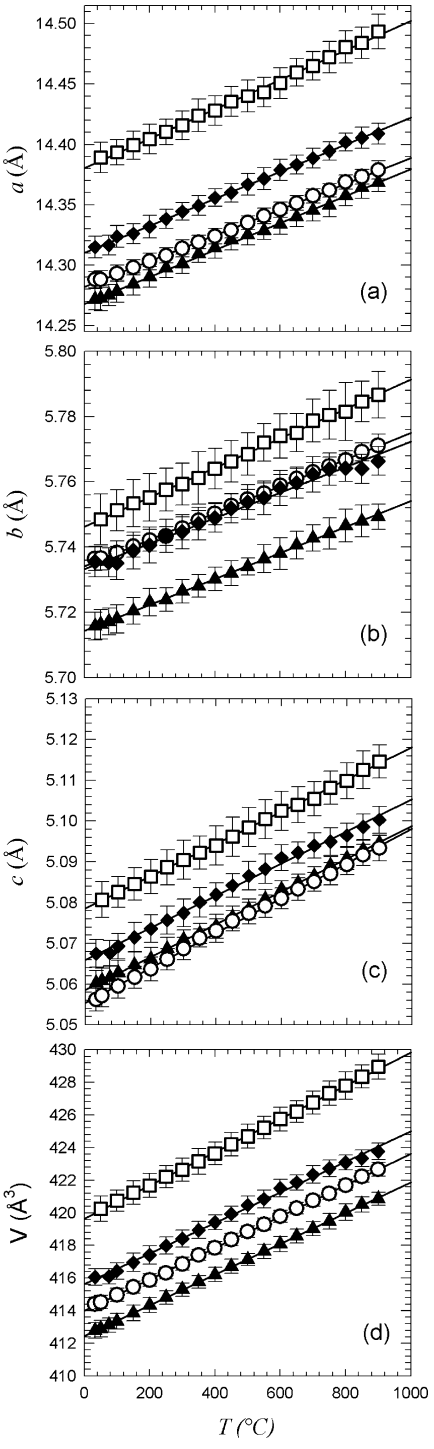

Fig. 1a–d Variation of unit-cell parameters with temperature for columbites. **a** *a* vs. *T*; **b** *b* vs. *T*; **c** *c* vs. *T*; **d** *V* vs. *T*. *Open circles* Col BRA N.3; *triangles* Col AMB N.1; *diamonds* Col AMB N.12; *open squares* Col KRA N.5. Linear regressions are reported as *solid lines*. 1σ error bars are reported

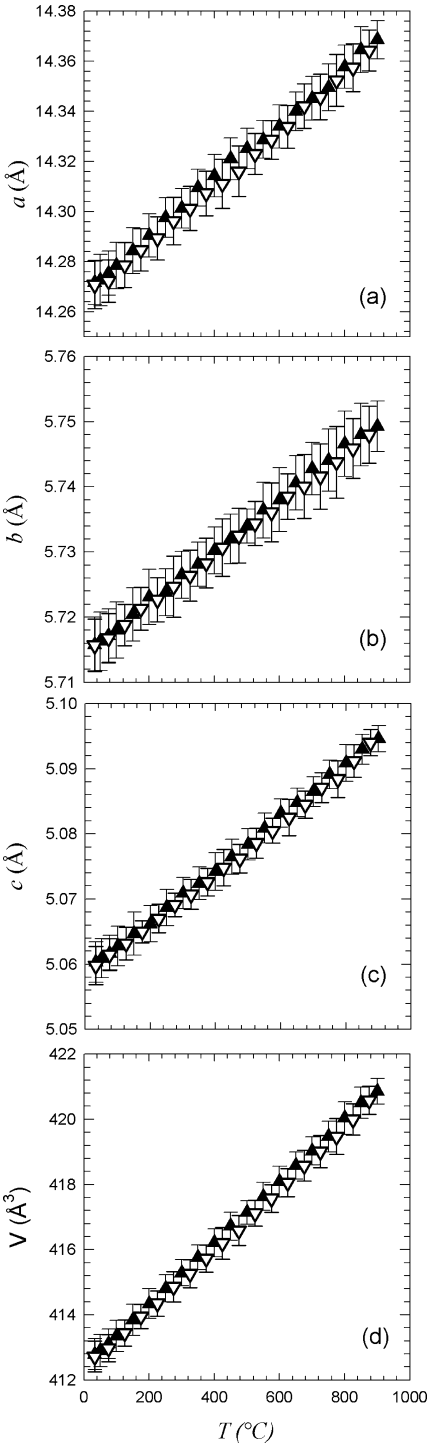

Fig. 2a–d Variation of unit-cell parameters with temperature for crystal Col AMB N.1 under heating-up (*triangles up*) and cooling-down (*open triangles down*) conditions. **a** *a* vs. *T*; **b** *b* vs. *T*; **c** *c* vs. *T*; **d** *V* vs. *T*. 1σ error bars are reported

the same distance with increasing T, Mn^{2+} being larger than Fe^{2+}.

The average <B–O>bond lengths show a slight, linear increase as a function of temperature (Fig. 3b). Although the B site is occupied in the two samples by the same pentavalent cations, the slope of the linear regression is larger for the KRA sample. This difference may be due to the larger size-mismatch in manganocolumbite between A and B sites, giving the latter more scope for expansion at high temperatures. Hence, in

Table 11 Structural thermal expansion of natural columbites. Standard deviation are given in parentheses

Sample	Expansion coefficients ($\times 10^{-6}$ K^{-1})					Anisotropy factor A^b
	a-axis α (*a*)	*b*-axis α (*b*)	*c*-axis α (*c*)	Mean $\bar{\alpha}^a$	Volume α(V)	
Col BRA N.3	6.98(23)	6.64(29)	8.64(27)	7.42(10)	22.2(3)	3.99(1.06)
Col AMB N.12	7.52(16)	6.43(35)	7.58(27)	7.18(22)	21.7(7)	2.45(0.50)
Col AMB N.1	7.89(26)	6.90(25)	7.69(24)	7.50 (4)	22.7(1)	2.21(0.67)
Col KRA N.5	7.87(40)	7.65(27)	7.67(16)	7.73(16)	23.4(6)	0.99(0.47)

[a] Mean thermal expansion coefficient is given by $\bar{\alpha} = [\alpha(a) + \alpha(b) + \alpha(c)]/3$
[b] Anisotropy factor A of thermal expansion is given by $A = [|\alpha(b) - \alpha(a)| + |\alpha(b) - \alpha(c)| + |\alpha(c) - \alpha(a)|] \times 10^{-6}$

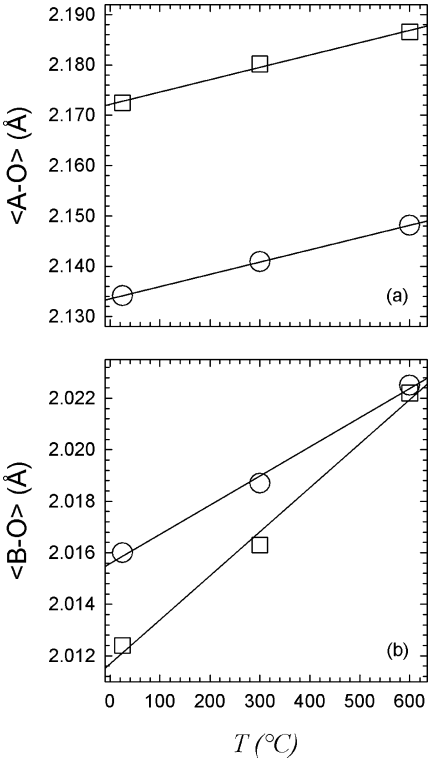

Fig. 3a–b Variation of octahedral mean bond distances as a function of temperature. **a** <A–O>vs. *T*; **b** <B–O>vs. *T*. *Open squares* Col KRA N.5; *open circles* Col BRA N.3

manganocolumbite, expansion along the direction of stacking of the ABB layers (*a* axis) is larger than in ferrocolumbite, as evident from data in Table 11. The shape and the internal distortion of the B polyhedron do not change in response to thermal treatments.

In conclusion, thermal expansion of the columbite structure occurs preferentially along the *a* and *c* directions, the former being the direction of stacking of the ABB layers, and the latter the direction of extension of the chains. The *b* direction, along which polyhedra belonging to different chains are joined through the sharing of corners, is the less favourite direction. It is worth noting that in ferrocolumbite, due to the smaller size of the A site, expansion is larger in the direction along which the chains extend (*c* axis), while in manganocolumbite, the larger size-mismatch between A and B sites induces the structure to expand significantly also along the *a* direction and the structure results almost isotropic with respect to thermal expansion.

Acknowledgements The authors thank Prof. O. Grubessi, Dr. L. Marino (University of Rome), Prof. C. Cipriani and Dr. G. Mazzetti (University of Florence) for providing the samples. Dr. Simona Bigi is thanked for microprobe analyses; funding by CNR is also acknowledged. Thanks to T.S. Ercit for his insightful comments on the manuscript. Financial support was provided by the Italian MURST project Structural evolution and phase transitions in minerals versus temperature, pressure and composition.

References

Blessing RH (1995) An empirical correction for absorption anisotropy. Acta Crystallogr (A) 51: 33–38
Blessing RH, Coppens P, Becker P (1974) Computer analysis of step-scanned X-ray data. J Appl. Crystrallogr 7: 488–492
Cannillo E, Germani G, Mazzi F (1983) New crystallographic software for Philips PW 1100 single-crystal diffractometer. CNR Centro di Studio per la Cristallografia, Internal Report 2
Černý P, Turnock AC (1971) Niobium–tantalum minerals from granitic pegmatites at Greer Lake, southeastern Manitoba. Can Mineral 10: 755–772
Černý P, Ercit TS (1985) Some recent advances in the mineralogy and geochemistry of Nb and Ta in rare-element granitic pegmatites. Bull Minéral 108: 499–532
Černý P, Goad BE, Hawthorne FC, Chapman R (1986) Fractionation trends of the Nb- and Ta-bearing oxide minerals in the Greer Lake pegmatitic granite and its pegmatite aureole, southwestern Manitoba. Am Mineral 71: 501–517
Donovan JJ, Rivers ML (1990) PRSUPR – a PC based automation and analysis software package for wavelength-dispersive electron-beam microanalysis. Microbeam Anal 66–68
Ercit TS (1994) The geochemistry and crystal chemistry of columbite group granitic pegmatites, southwest Grenville Province, Canadian Shield. Can Mineral 32: 421–438
Ercit TS, Wise MA, Černý P (1995) Compositional and structural systematics of the columbite group. Am Mineral 80: 613–619
Griffen DH, Ribbe PH (1979) Distortion in the tetrahedral oxyanions of crystalline substances. N J Mineral Abh 137: 54–73
Ibers JA, Hamilton WC (1974) International tables for X-ray crystallography vol 4. Kynoch Press, Birmingham, UK, pp 99–101
Komkov AI (1970) Relationship between the X-ray constants of columbites and composition. Døkl Akad Nauk SSSR 195: 117–119
Lahti SI (1987) Zoning in columbite-tantalite crystals from the granitic pegmatites at Eräjärvi area, southern Finland. Geoch Cosmoch Acta 51: 509–517
Lehman MS, Larsen FK (1974) A method for location of the peaks in step-scan measured Bragg reflections. Acta Crystallogr (A)30: 580–584

Mulja T, Williams-Jones AE, Martin RF, Wood SA (1996), Compositional variation and structural state of columbite-tantalite in rare-element granitic pegmatites of the Preissac-Lacorne batholith, Quebec, Canada. Am Mineral 81: 146–157

Nickel EH, Rowland JF, McAdam RC (1963) Ixiolite – a columbite substructure. Am Mineral 48: 961–979

North ACT, Phillips DC, Mathews FS (1968) A semi-empirical method of absorption correction. Acta Crystrallogr (A) 24: 351–359

Sheldrick GM (1996) SADABS. Institüt für Anorganische Chemie der Universität, Göttingen, Germany

Sheldrick GM (1998) SHELX97 – Programs for crystal structure analysis (release 97–2). Institüt für Anorganische Chemie der Universität, Göttingen, Germany

Schneider H, Eberhard E (1990) Thermal expansion of mullite. J Am Ceram Soc 73: 2073–2076

Trueman DL, Černý P (1982) Exploration for rare-element granitic pegmatites. In: Mineralogical Association of Canada Short Course Handbook 8: 463–491

Turnock AC (1965) Synthetic wodginite, tapiolite and tantalite. Can Mineral 8: 461–470

Wise MA, Turnock AC, Černý P (1985) Improved unit-cell dimensions for ordered columbite–tantalite end members. N Jb Miner Mh 8: 372–378